ELSEVIER

Physica E 6 (2000) 358–363

PHYSICA E

www.elsevier.nl/locate/physe

Vertical quantum dots at high magnetic fields beyond the few-electron limit

D.G. Austing[a,*], Y. Tokura[a], S. Tarucha[a,b], T.H. Oosterkamp[c], J.W. Janssen[c], M.W.S. Danoesastro[c], L.P. Kouwenhoven[c]

[a] *NTT Basic Research Laboratories, 3-1 Wakamiya, Morinosato, Atsugi, Kanagawa 243-0198, Japan*
[b] *Department of Physics, University of Tokyo, 7-3-1 Hongo, Bunkyo-ku, Tokyo 113-0033, Japan*
[c] *Department of Applied Physics and DIMES, Delft University of Technology, PO Box 5046, 2600 GA Delft, Netherlands*

Abstract

We describe phenomena that can be studied in vertical quantum dot single electron transistors. Moving from the *few*-electron to the *several*- and *many*-electron regimes, features in the conductance peaks initially related to spin polarization evolve with magnetic field. This allows us to first probe the spin-flip region beyond the last single-particle crossing at low field, and then the formation and stability of the spin-polarized maximum density droplet at high field. According to a simple capacitance model, charge redistribution in the dot at higher magnetic fields is accompanied by abrupt changes in the area of the droplet.

PACS: 85.30.Vw; 73.20.Dx; 79.60.Jv; 85.30.Wx

Keywords: Quantum dots; Artificial atom; Spin-flip; Maximum density droplet

Single electron phenomena in quantum dots continue to attract attention [1–3]. We have reported atomic-like properties of well-defined vertical quantum dot disks [4,5]. For a small DC source-drain voltage applied across the dot, V_{SD}, ground states have been probed in the linear response regime when the number of electrons trapped on the dot, N, is between 0 and 20 for a magnetic (B-) field up to 3.5 T by measuring the current, I, flowing through the dot as a function of voltage, V_g, applied to a single Schottky gate [4]. With a finite V_{SD}, and measuring current stripes instead of current peaks, the first few excited states can also be accessed in the non-linear response regime in the few-electron limit ($N < 6$) for B-fields up to 16 T [5].

We expand our recent studies to probe features, which show up strikingly in a B–N phase diagram beyond the few-electron regime [6,7]. Because of the reduction of the lateral confinement and the increase in screening as N increases, a two-dimensional limit is approached for large N. In the presence of a B-field, which strengthens electron interactions, we see

* Corresponding author. Tel.: ++81-462-40-3479; fax: ++81-462-40-4723.
E-mail address: austing@will.brl.ntt.co.jp (D.G. Austing)

1386-9477/00/$ - see front matter
PII: S1386-9477(99)00169-1

features related to those familiar in the quantum Hall regime for a two-dimensional electron gas (2DEG), and the concept of a filling factor, ν, becomes useful. Features which can be fully explained by many-body calculations up to $N = 5$ in the few-electron regime [5], extend in to the several- and many-electron regimes and reflect a larger dot with a more 2D character. As the B-field is increased beyond that required to achieve $\nu = 2$, from 'cusps' and 'steps' in the position of the conductance peaks, we identify the spin-flip regime before the formation at $\nu = 1$ of a maximum density droplet (MDD)- so called because it is the densest spin-polarized electron configuration allowed by the available quantum states [8]. Until now, only two-terminal capacitance–voltage measurements have permitted access to the interesting physics at high B-fields in a vertical quantum dot [1,2].

The material is a specially designed double barrier structure with an $In_{0.05}Ga_{0.95}As$ well, $Al_{0.22}Ga_{0.78}As$ barriers, and n-doped GaAs contacts [4], which is processed to form circular mesas by a special etching technique, and a gate is placed around each dot-mesa [9,10]. We discuss two devices A and B which both have a geometrical diameter of 0.54 μm. Measurements on devices A and B are performed in a dilution refrigerator and in a ^{3}He cryostat, respectively. The B-field is applied parallel to the current. N typically varies from several tens at $V_g = 0$ V to zero at the 'pinch-off' voltage (≈ -2 V).

Fig. 1 shows the current peaks versus B for device A for N from 0 to 18 up to 14 T. On making V_g more positive, peaks are measured for every extra electron that enters the dot. At 0 T, a shell structure for a 2D harmonic potential is observed in the addition energy (large peak spacings for $N = 2, 6, 12$), and Hund's first rule explains the relatively large peak spacing for $N = 4$. Peaks evolve in pairs for $B < 2$ T, implying that each single-particle state is filled with two electrons of opposite spin [4]. "Wiggles" indicate crossings between single-particle states. For $N > 4$, the last "wiggle" identifies when all electrons occupy spin-degenerate states belonging to the lowest orbital Landau level which corresponds to $\nu = 2$ in a 2DEG. This means that for even-N, the ground state is spin-unpolarized (total spin, S, is 0), and the total angular momentum, M, is $N(N-2)/4$.

In the constant interaction model, no transitions in the ground states beyond $\nu = 2$ are expected if

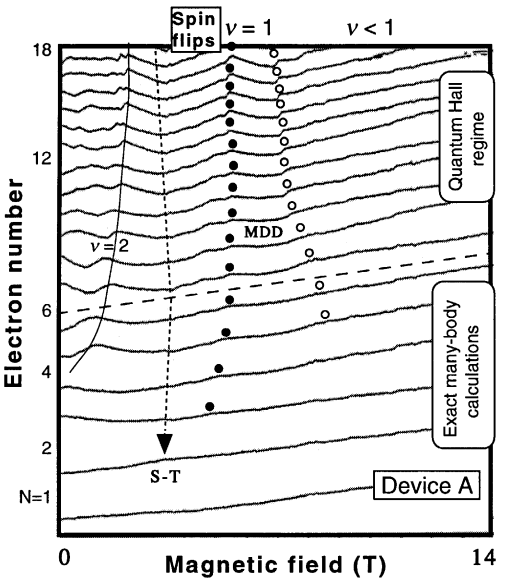

Fig. 1. B–N phase diagram for device A. V_{SD} is ≈ 100 μV. The positions of the conductance peaks reflecting the N-electron ground states is built-up of many current traces versus V_g (from -2.1 to -0.8 V) that have been offset by a value proportional to B. The solid (open) dots mark the beginning (end) of the MDD. The singlet–triplet (S–T) transition for $N = 2$ is identified by ▼.

the weak Zeeman effect is neglected. However, in the presence of many-body effects, transitions in the N-electron ground states occur in such a way that M is increased, and S is maximized. The former is favored by the direct Coulomb energy and influenced by the kinetic energy, whilst the latter is favored by exchange and Zeeman energies, and modified by correlation effects [11–20]. Beyond $\nu = 2$, according to a simple self-consistent model introduced for planar-dots containing several-electrons [21,22], it is energetically favorable for minority spin-down electrons at the compressible dot center to sequentially tunnel through an incompressible 'ring' to the compressible dot edge so becoming majority spin-up electrons. Spin-flip processes have been studied experimentally in planar dots [21–26], and theoretically [26–29].

For $N < 6$, we have measured current peaks and stripes to track the transitions beyond $\nu = 2$ [5]. Our spectra compare well with those calculated incorporating many-body effects, so we can confidently identify the configurations of the ground and first few

excited states. In Fig. 1, ▼ locates the position of the singlet–triplet (S–T) transition for $N = 2$ [11,12]. In a single spin-flip process, both S and M simultaneously change from 0 to 1, and the 2-electron system becomes spin-polarized. For $N > 2$ the process of spin-polarization occurs over a finite B-field range. Weak features mark where this process occurs. At B-fields marked by ▼ and ●, the N-electron system has become completely spin-polarized. S is $N/2$ and M is $N(N-1)/2$. Not all the predicted transitions can readily be observed, and not all transitions actually involve a spin-flip (although one naively expects for even-N and odd-N, respectively, $N/2$ and $(N-1)/2$ spin-flips) [6].

For device B, there seem to be just one or two weak features in the spin-flip regime for N from 5 to about 10 [6], and their number does not clearly increase with N, so not all the expected transitions for $2 > \nu > 1$ can yet be readily distinguished. Crucially, N may not be sufficiently large that compressible and incompressible regions can meaningfully be defined in the still quite small dot. Many-body states are still expected to be important, and B-field-induced transitions are presumably responsible for the weak features, although the states cannot be labeled at present. Increasing N, into the several-electron regime, N is sufficiently large that the simple self-consistent model should be helpful [21,22]. Fig. 2(a) shows the B–N phase diagram for $N \approx 25$. Beyond $\nu = 2$, there is a sequence of six or seven features (solid squares) before the final feature at ≈ 6.2 T marking $\nu = 1$. The shape of the features changes from 'cusp'-like at low field to 'step'-like and even 'peak'-like at high field. The number of features still does not obviously increase with N for consecutive peaks. Compressible and incompressible regions within the dot should have formed, and the MDD should be clear, but still we can expect a small but finite excitation energy in the single-particle picture, and many-body states are probably not yet negligible. Increasing N further, we move into the many-electron regime. Fig. 2(b) shows the B–N phase diagram for $N \approx 45$. Beyond $\nu = 2$, there is a string of about nine or ten features (solid ovals) before the last feature at ≈ 6.2 T marking $\nu = 1$. Compressible and incompressible regions inside the dot, and the MDD should now be very well established. Many-body states are now not expected to be important. The features in Fig. 2(b) are similar to those in Fig. 2(a), but yet again

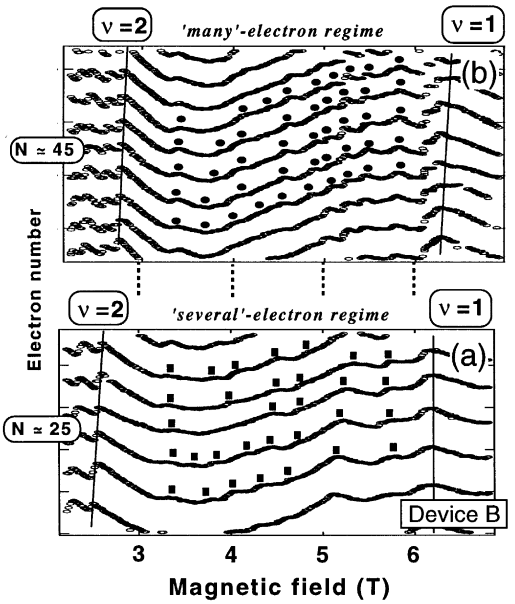

Fig. 2. B–N phase diagram for device B in the spin-flip regime between $\nu = 2$ and $\nu = 1$ in the region of (a) $N \approx 25$ and (b) $N \approx 45$. V_{SD} is ≈ 30 μV.

the number of features does not really increase with N for successive peaks, and their number is certainly a lot less than $N/2$.

Naively, one expects the simple self-consistent model [21,22] to be applicable, and yet based on our observations, and the capacitance–voltage data of Ashoori [1,2], the appearance of the spin-flips, and their numbers are very different in vertical dots compared to planar dots, i.e. geometry is important. The influence of the emitter in the former is not well understood. It is probable that at low B-fields ($\nu \approx 2$) there are incomplete edge states in the emitter, so the complex nature of these states and how they couple to dot states across the emitter barrier could strongly influence the spin-flips. In contrast, $N/2$ oscillations in the position of each peak for planar dots are well resolved [21–26], because the edge states in the emitter are well defined, and the current is carried principally by the strong coupling of these states to nearby edge states in the dot. We note that in subsequent work on planar dots, the self-consistent model was superceded by other more advanced models [24–26] to explain important experimental observations [21–26].

Returning to Fig. 1, after the last spin-flip, for $N > 2$, solid circles mark the beginning of the spin-polarized MDD (which for $N = 2$ is the S–T transition identified by ▼), and open circles seem to mark the end of the MDD. Solid circles actually identify $\nu = 1$, and the beginning of a distinct MDD phase in which all N-electrons are in the lowest Landau level, and all successive single-particle states $(n, \ell) = (0,0),(0,1),\ldots,(0,N-1)$ are occupied by one spin-up electron (n and ℓ, respectively, are the radial and angular momentum quantum numbers for a 2D harmonic potential) [8]. The stability of the MDD as the B-field is further increased is set by the balance of forces acting on this finite electron system [8,30–35]; namely, the inward force of the confining potential, the repulsive force of the direct Coulomb interaction between electrons, and a binding force due to the exchange interaction. In addition, Zeeman energy and correlation effects are important. As the B-field and the electron number are changed, the relative strength of these forces is tuned, which induces transitions between the MDD and other states [1,2,24–26].

As N increases, the start of the MDD first moves to larger B and then becomes roughly independent of N. As the B-field is increased further, the angular momentum states shrink in size such that the density of the MDD increases. At some threshold (identified by ◯), the direct Coulomb interaction becomes so large that the MDD breaks apart into a larger lower density droplet (LDD). Assuming the LDD remains spin-polarized, successive angular momentum states are no longer occupied, i.e. $M > N(N-1)/2$. Whether the unoccupied states are in the center [8], or at the edge [35], depends critically on the relative strengths of the confinement, exchange, and direct Coulomb interactions, as well as the Zeeman energy and correlation effects. It has been suggested, especially when the Zeeman energy is small, that the MDD may even become unstable towards the formation of spin-texture [36,37]. The stability conditions for the MDD (i.e. the B-range between ● and ◯) has been calculated by several different theoretical approaches with different assumptions [8,30–35]. One recent spin-density functional calculation predicts left and right boundaries for the MDD that are strikingly similar to those in Fig. 1 [38]. It is nonetheless challenging to make good quantitative comparisons, since

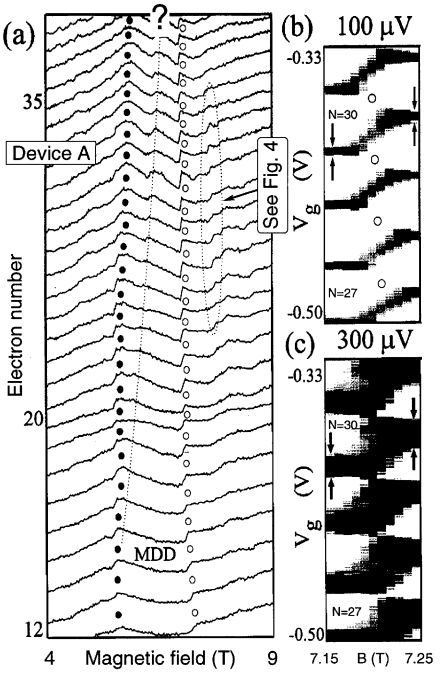

Fig. 3. (a) Peak positions versus B for device A for $N = 12$ to 39 extracted from many current traces (V_g is from -0.9 to -0.1 V). ● and ◯ mark the same transitions as in Fig. 1. Additional transitions beyond the open circles are indicated (see Fig. 4). Greyscale plots, (b) and (c), of I versus V_g for B-values in a small interval around steps marked by ◯. V_{SD} is 100 μV in (b) and 300 μV in (c).

the phase diagrams are very sensitive to the finite thickness of the dot and to screening effects from electrons in the contacts.

Fig. 3(a) shows the peak positions versus B-field for device A for $N > 11$. Between the boundaries marked by ● and ◯ a new transition seems to develop for $N > 15$, and indicates a new electronic configuration inside this region (see dotted line). We believe the MDD continues on the right of this new transition but, since we cannot identify the new state on the left, this is debatable. At this moment no calculations exist for our specific sample. Intriguingly, kinks in the peak evolution marking the boundaries of the MDD for small N turn into abrupt steps for $N \gtrsim 10$. This is also true for the new unidentified transition as N is increased, and also at higher B-fields, e.g. in region marked by the dotted oval, additional steps can be discerned in Fig. 3(a). We argue that at all these steps,

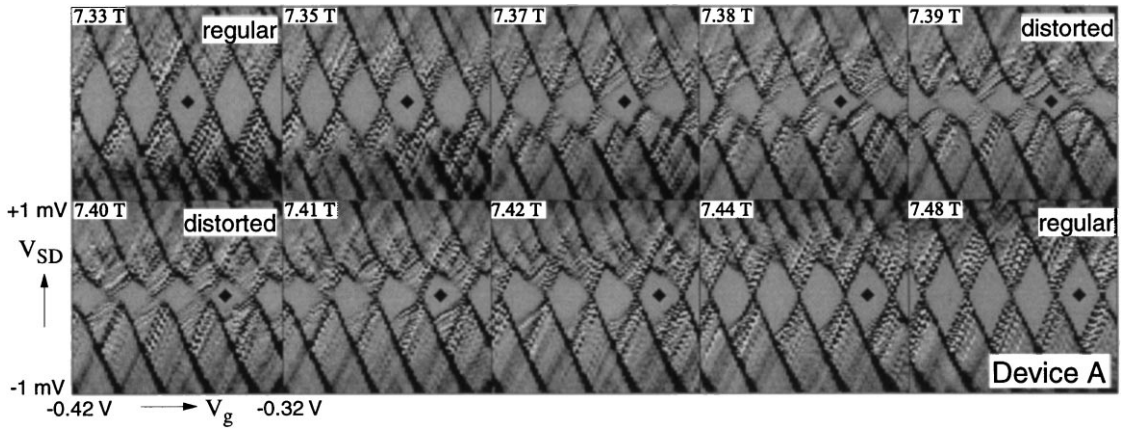

Fig. 4. Grey-scale plots of dI/dV_{SD} in the V_g–V_{SD} plane (-1 mV $< V_{SD} < +1$ mV and -0.42 V $< V_g < -0.32$ V) for device A for ten B-values before, during, and after a sequence of steps beyond the open circles as indicated in Fig. 3(a). $N = 31$ is marked by ♦. The regular Coulomb blockade regions at the lowest and highest B-field have the familiar shapes, but in between, they are severely distored.

the charge distribution of the droplet changes abruptly. Figs. 3(b) and (c) show I versus V_g (N=27–31) in grey scale for B-values around the steps marked by ◯. The step width is about 50 mT. For $V_{SD} = 100$ μV, the peaks are much narrower than their spacings. An increased source-drain voltage $V_{SD} = 300$ μV broadens these peaks. The important point is that the peak width, ΔV_g, increases by about 10% after crossing the step as indicated by the arrows. At low temperature $\alpha \Delta V_g = eV_{SD}$, where according to a simple capacitance model $\alpha = eC_g/C_\Sigma$. As the total capacitance, C_Σ, in our geometry is roughly proportional to the dot area, and since the gate capacitance C_g increases only slowly with the dot area, the change in peak width implies that the dot area changes abruptly by about 10%. However, it is not clear how well the MDD state can be modeled by capacitances. It is also evident in Figs. 3(b) and (c) that the peak width during the step is about twice the width outside the step region. All steps show similar behavior.

To study the nature of these unusual steps we have measured excitation spectra. Fig. 4 shows dI/dV_{SD} in the V_{SD}–V_g plane for ten B-values around a particular step that separates two different LDD states in the B-field regime within the dotted oval in Fig. 3(a). We again stress that the same behaviour is found at all steps. At the lowest and highest B-fields the Coulomb blockade regions have the expected diamond shape, but the diamond at $B = 7.48$ T is about 10% smaller in the V_{SD} direction, indicating that the energy to overcome the Coulomb gap has decreased by ≈ 10%. This is again consistent with $a \approx 10\%$ larger dot area after the charge redistribution. Strikingly, the shape of the diamonds measured inside the step region is severely distorted, where the size of the Coulomb blockade region collapses to as little as ≈ 40% of its value outside the step region. This agrees with the peak broadening by about a factor of 2 during the steps in Figs. 3(b) and (c). We are not aware of such a collapse of the Coulomb gap in metallic or semiconducting systems. Elsewhere, we outline how the distorted and collapsing Coulomb blockade regions can be obtained within a simple phenomenological model in which a set of parabolas representing one charge configuration (e.g. the MDD) is gradually displaced relative to another set of parabolas representing a different charge configuration (e.g. the LDD) [7]. From this we again conclude that the instability of the MDD and the instability of LDD states at higher B-fields are accompanied by a redistribution of charge. It remains a challenge, however, to calculate the microscopic origin of the different in offset charge between two states with different charge distributions.

Acknowledgements

We gratefully acknowledge the considerable assistance of T. Honda in the fabrication of the devices.

We also thank G. Bauer, S. Cronenwett, M. Devoret, L. Glazman, R. van der Hage, J. Mooij, K. Muraki, Yu. Nazarov, and S.J. Tans for experimental help and discussions. The work was supported by the Dutch Foundation for Fundamental Research on Matter (FOM), and by the NEDO joint research program (NTDP-98).

References

[1] R.C. Ashoori, Nature 379 (1996) 413.
[2] R.C. Ashoori et al., Phys. Rev. Lett. 71 (1993) 613.
[3] U. Meirav, E.B. Foxman, Semicond. Sci. Technol. 11 (1996) 255.
[4] S. Tarucha et al., Phys. Rev. Lett. 77 (1996) 3613.
[5] L.P. Kouwenhoven et al., Science 278 (1997) 1788.
[6] D.G. Austing et al., Jpn. J. Appl. Phys. 38 (1999) 372.
[7] T.H. Oosterkamp et al., Phys. Rev. Lett. 82 (1999) 2931.
[8] A.H. MacDonald et al., Aust. J. Phys. 46 (1993) 345.
[9] D.G. Austing et al., Jpn. J. Appl. Phys. 34 (1995) 1320.
[10] D.G. Austing et al., Semicond. Sci. Technol. 11 (1996) 388.
[11] M. Wagner et al., Phys. Rev. B 45 (1992) 1951.
[12] D. Pfannkuche et al., Phys. Rev. B 47 (1993) 2244.
[13] P.A. Maksym, T. Chakraborty, Phys. Rev. Lett. 65 (1990) 108.
[14] P.A. Maksym, T. Chakraborty, Phys. Rev. B 45 (1992) 1947.
[15] P. Hawrylak, Phys. Rev. Lett. 71 (1993) 3347.
[16] S.-R.E. Yang et al., Phys. Rev. Lett. 71 (1993) 3194.
[17] M. Ferconi, G. Vignale, Phys. Rev. B 50 (1994) 14 722.
[18] J.J. Palacios et al., Phys. Rev. B 50 (1994) 5760.
[19] M. Eto, Jpn. J. Appl. Phys. 36 (1997) 3924.
[20] A. Harju et al., Phys. Rev. B 59 (1999) 5622.
[21] P.L. McEuen et al., Phys. Rev. B 45 (1992) 11 419.
[22] P.L. McEuen et al., Physica B 189 (1993) 70.
[23] N.C. van der Vaart et al., Phys. Rev. Lett. 73 (1994) 320.
[24] O. Klein et al., Phys. Rev. Lett. 74 (1995) 785.
[25] O. Klein et al., Phys. Rev. B 53 (1995) R4221.
[26] P. Hawrylak et al., Phys. Rev. B 59 (1999) 2801.
[27] A.K. Evans et al., Phys. Rev. B 48 (1993) 11 120.
[28] J.H. Oaknin et al., Phys. Rev. B 49 (1994) 5718.
[29] T.H. Stoof, G.E.W. Bauer, Phys. Rev. B 52 (1995) 12 143.
[30] J.H. Oaknin et al., Phys. Rev. Lett. 74 (1995) 5120.
[31] K.-H. Ahn et al., Phys. Rev. B 52 (1995) 13 757.
[32] M. Ferconi, G. Vignale, Phys. Rev. B 56 (1997) 12 108.
[33] A. Wojs, P. Hawrylak, Phys. Rev. B 56 (1997) 13 227.
[34] M. Eto, Jpn. J. Appl. Phys. 38 (1999) 376.
[35] C. de C. Chamon, X.G. Wen, Phys. Rev. B 49 (1994) 8227.
[36] A. Karlhede et al., Phys. Rev. Lett. 77 (1996) 2061.
[37] J.H. Oaknin et al., Phys. Rev. B 54 (1996) 16 850.
[38] S.M. Reimann et al., Phys. Rev. Lett. 83 (1999) 3270.